Applied Catalysis B: Environmental 313 (2022) 121448

Contents lists available at ScienceDirect

Applied Catalysis B: Environmental

journal homepage: www.elsevier.com/locate/apcatb

Transient kinetic analysis of passive SCR systems for NH_3 abatement from natural gas fueled heavy duty engines over dual-layer ASC catalysts: An experimental and modelling study

Nicola Usberti [a], Sara Ciria [a], Stefano Golini [b], Gabriella Mancino [b], Edoardo Merlone Borla [b], Isabella Nova [a], Enrico Tronconi [a,*]

[a] Laboratory of Catalysis and Catalytic Processes, Dipartimento di Energia, Politecnico di Milano, Via La Masa 34, 20156 Milano, Italy
[b] FPT Industrial S.p.a., via Puglia 15, 10156 Torino, Italy

ARTICLE INFO

Keywords:
Passive SCR
ASC dual-layer catalyst
NH_3 abatement
NH_3 slip
Pt/Al_2O_3
Cu zeolite

ABSTRACT

Air-to-fuel ratios fluctuating around the stoichiometric value enable the best CH_4, NO_X and CO abatement performance of the three-way catalytic converters implemented in NGVs after-treatment systems; however, this leads to undesired NH_3 production and potential slip under rich combustion conditions. An additional Passive SCR catalytic device placed downstream of the TWC, based on a dual-layer SCR+PGM configuration, could represent the solution.

Through both transient experimental tests and modelling analysis, we demonstrate that effective NH_3 abatement is achieved at low temperatures by its adsorption onto the SCR catalyst during the rich phases, and its further consumption by $NO+O_2$ under lean conditions. Differently, at high temperatures NH_3 is efficiently and selectively converted to nitrogen by direct oxidation through a redox reaction mechanism. The developed model can predict the performances of both fresh and aged catalysts under the transient rich-lean cycling experimental conditions investigated.

1. Introduction

In recent years, the pressing demand of finding alternative energy sources and the implementation of progressively more stringent pollutants emissions regulations have dramatically changed the global automotive industry market [1]. Although nowadays the road transport fleet is still dominated by liquid fossil fuels powered vehicles, natural gas (NG) has attracted significant attention as an alternative fuel (in particular for heavy-duty vehicles) due to its easy availability, cheaper price compared to diesel or gasoline and technological maturity [2–4]. Its chemical composition (mostly CH_4, mixed with smaller contents of short-chain hydrocarbons, such as C_2H_6, C_3H_8 and C_4H_{10}, up to 20% [5]) enables reduced emissions of CO_X, due to its lower C/H ratio compared to traditional liquid fuels [2,3], of NO_X, due to its higher flame stability and lower combustion temperature [3,6], and of S-containing pollutants, due to its lower sulphur content. On the other hand, methane has a greenhouse effect 25 times higher than CO_2 [7] and, thus, its emissions are strictly controlled and limited by current regulations. Regarding natural gas fueled vehicles (NGVs), noble metals (typically Pt, Pd and/or Rh) based three-way catalyst (TWC) converters implemented in the exhaust gases after-treatment systems are the state of art technology for unburned methane abatement, as well as simultaneous oxidation of CO to CO_2 and reduction of NO_X to N_2 and H_2O [8,9]. Developed and applied since the 1970s for the abatement of unburned hydrocarbons from lean-burn gasoline engines [3,10,11], three-way catalysts and their performance are deeply studied in the literature: several papers reported that, under realistic NGVs exhaust gases operating conditions, CH_4 and NO_X conversions over commercial TWC catalysts are strongly affected by the oscillating air to fuel ratios (ATRs) characterising the engine combustion, rapidly and periodically switching (a process called lean-rich dithering) from rich (sub-stoichiometric equivalent air to fuel ratio) to lean conditions (over-stoichiometric equivalent air to fuel ratio) [12–16]. In particular, it was found that the maximum catalytic performance can be achieved by maintaining an average λ (calculated parameter describing the ATRs) corresponding to stoichiometric or slightly rich conditions [14,15]. In fact, in the absence of oxygen, methane (and other hydrocarbons) and NO_X are converted respectively by steam reforming and reactions with H_2 and CO [3,17,18]; the

* Corresponding author.
E-mail address: enrico.tronconi@polimi.it (E. Tronconi).

https://doi.org/10.1016/j.apcatb.2022.121448
Received 29 October 2021; Received in revised form 22 April 2022; Accepted 23 April 2022
Available online 28 April 2022

mechanism is completed by the water gas shift equilibrium. The stoichiometries of the cited reactions are listed below:

Water gas shift reaction:

$$CO + H_2O \leftrightarrow CO_2 + H_2 \quad \text{(R1)}$$

Methane and other hydrocarbons steam reforming:

$$CH_4 + H_2O \rightarrow CO + 3H_2 \quad \text{(R2)}$$

$$C_nH_m + nH_2O \rightarrow nCO + \left(\frac{m}{2} + n\right)H_2 \quad \text{(R3)}$$

NO reduction reactions:

$$NO + H_2 \rightarrow \frac{1}{2}N_2 + H_2O \quad \text{(R4)}$$

$$NO + CO \rightarrow \frac{1}{2}N_2 + CO_2 \quad \text{(R5)}$$

$$4NO + CH_4 \rightarrow 2N_2 + CO_2 + 2H_2O \quad \text{(R6)}$$

Under rich conditions (without O_2), a significant amount of H_2 is produced on the TWC by the steam reforming of unburned methane (R2) and other hydrocarbons (R3) and the water gas shift reactions (R1), allowing the onset of R4, R5 and R6 and thus leading to the consumption of NO_X.

Although under reducing operating conditions (rich combustion exhaust gases), TWC methane and NOx abatement performance are better compared to lean combustion conditions (O_2 rapidly converts the produced H_2 and CO), a significant drawback is the well documented ammonia (NH_3) formation on the catalytic converter [19–22]. This happens because, in the TWC, the effective reactions not only include the reduction of NO_X to N_2, but also the formation of other nitrogen species, such as ammonia, following reactions R7 and R8.

$$2NO + 5H_2 \rightarrow 2NH_3 + 2H_2O \quad \text{(R7)}$$

$$2NO + 4CO + 2H_2O + H_2 \rightarrow 2NH_3 + 4CO_2 \quad \text{(R8)}$$

Ammonia is known for its toxicity and instability, so its emissions are strictly regulated by current legislations. NH_3 production on the TWC converter significantly depends on the engine operating parameters, such as air to fuel ratio, engine speed and engine load. Prikhodko et al. [21], by means of steady-state tests performed under realistic gasoline fueled engine out exhaust gases compositions (unburned HC, NOx, CO, H2, O_2), demonstrated almost complete NOx conversions, but very high ammonia yields under rich combustion conditions (fuel excess in respect with oxygen), thus with air to fuel ratios less than one: for example, these authors reported ammonia yields close to 100% with respect to inlet NOx for air to fuels ratios of 0.96 and lower, with concentrations higher than 1000 ppm of NH_3 detected at reactor outlet. Approaching stoichiometric and further lean conditions, ammonia formation and NOx conversion drastically dropped through TWC. Similar trends were confirmed by Zhang et al. [23], who studied ammonia formation on TWC converters implemented in NGVs after-treatment systems with steady-state tests and more realistic engine homologation test cycles (WHTC, world harmonized transient cycles): under these conditions, the authors reported average NH_3 emissions of 109 and 120 ppm during cold and hot transient cycles, respectively, concentrated in sudden and sharp peaks of 500 ppm and higher, corresponding to high engine loads and low oxygen content in the exhaust gases. It is also important to note the effect of temperature on ammonia production during engine test cycles: generally, as demonstrated by the difference in the averages between cold and hot cycles, higher temperatures result in higher TWC activity and, thus, higher NH_3 production. Nevertheless, significant NH_3 emissions were also detected at the TWC outlet during the first part of the cold cycle (the so called cold-start transient of the engine), with exhaust gas temperatures of about 150 °C and higher. Finally, Pradham et al. [16] and Prikhodko et al. [24] also showed similar results, investigating the performance of TWC catalyst for natural gas- and gasoline-fuelled vehicles, respectively, in FPT (Federal Transient Procedure) driving cycles.

In order to reduce the ammonia slip, a possible solution is the implementation on the NGVs after-treatment train of an additional SCR converter, directly downstream the TWC [25,26]. This system (namely Passive SCR) should adsorb and convert the ammonia produced on the TWC under rich conditions through SCR DeNOx process (R9, R10) and, thus, improve the NO_X abatement activity of the after-treatment system.

$$NH_3 + \theta_{free} \leftarrow\rightarrow NH_3^* \quad \text{(R9)}$$

$$NH_3^* + NO + \frac{1}{4}O_2 \rightarrow N_2 + \frac{3}{2}H_2O \quad \text{(R10)}$$

In order to ensure efficient conversion of ammonia, the use of the single-layer SCR catalyst has been replaced by the use of the Ammonia Slip Catalyst (ASC) [19,27] for the Passive SCR converter. Typically, the ASC is characterized by a dual-layer configuration, with an inner noble metal-based oxidation catalytic layer (PGM, Pt as active element) and an external SCR catalytic layer (Cu- or Fe- exchanged zeolites). Unconverted ammonia diffuses through the SCR layer and reaches the Pt-based catalyst, extremely active in NH_3 oxidation reactions (stoichiometries reported in reactions R11 and R12).

$$NH_3^* + \frac{3}{4}O_2 \rightarrow \frac{1}{2}N_2 + \frac{3}{2}H_2O \quad \text{(R11)}$$

$$NH_3^* + \frac{5}{4}O_2 \rightarrow NO + \frac{3}{2}H_2O \quad \text{(R12)}$$

The overall N_2 selectivity is enhanced by the external SCR layer: NO_X species formed because of the unselective oxidations on the PGM layer diffuse back through the SCR layer above and get converted to N_2 by the residual ammonia.

The target of this work is the study of the NH_3 abatement and related DeNOx performance of a commercial ASC catalytic system under rich-lean cycling Passive SCR experimental conditions: by replicating the oscillating exhaust gases composition downstream the TWC due to the dithering process of the engine combustion (rich and lean conditions), we expect to collect significant experimental data to understand the Passive SCR NH_3 abatement mechanism and, thus, to develop a predictive model to accurately describe its activity.

Despite several works published on the modelling of dual-layer SCR catalytic systems [28,29], few contributions were directly addressed to the passive SCR topic and even less specifically to NH_3 and NO_X abatement from NGVs stoichiometric combustion exhaust gases. Recently, Chen and co-workers developed a predictive global model to evaluate and optimize the relation between NH_3 production over the TWC and passive SCR DeNOx efficiency for NOx abatement from lean-burn gasoline exhaust gases [25,26]. Alternatively, good accuracy in describing low temperature full-scale experimental data was achieved by Wang et al. [30], focusing on fresh and aged passive SCR catalysts ammonia adsorption capacity. Although these models resulted to be very effective under specific operating conditions, none of them really deals with the actual reaction mechanism, assessing for example what happens at high temperatures or during reactants concentration transients.

Starting from a series of experiments at both low and high temperatures, swapping from rich to lean conditions, we propose a suitable reaction mechanism and calibrate our model on the collected experimental data. Finally, the effect of the ageing process on the deNOx activity of the Passive SCR catalysts is investigated through a series of similar tests performed over two differently aged versions of the reference catalyst and incorporated in the model simulations.

2. Experimental

2.1. Catalysts

The experimental campaign was performed over washcoated monolith cores with square cross section (400 cpsi, 6×6 channels, length = 4 cm) of a fresh and two progressively aged samples of an industrial ASC catalyst, provided by FPT Industrial. This system was characterized by a dual-layer configuration, with an outer SCR layer including a state-of-the-art Cu-zeolite catalyst as active material and an inner PGM layer (Pt/Al_2O_3). The choice of Pt is due to its high ammonia oxidation activity [19,27]. The ageing of the monolith catalyst was performed at two different temperatures, respectively 750 °C and 850 °C, with 8% O_2 and 10% H_2O for 10 h: these are typical hydrothermal ageing conditions for SCR and Pt-based catalysts reported in literature [31–33] and, although not strictly representative of the field operating conditions of NGVs after-treatment systems (e.g. O_2 concentration effect), they cover the primary effect of temperature on the stability of the catalytic performance of the investigated system.

Table 1 provides specifications of the tested catalysts. The behavior of the dual-layer system, as well as the behaviors of the two individual system components, were found notably similar to those of typical ASC systems [28,34,35], Cu/CHA SCR catalysts [32,33,36–39], and PGM-based NH_3 oxidation catalysts [19,40], respectively, extensively described in the literature. In particular, the transient tests over our composite dual-layer system could be rationalized and modelled according to the known behavior of state-of-the-art Cu-SSZ-13 SCR catalysts with Cu/Al ratios = 0.15 – 0.30 and Si/Al ratios = 5 – 15 for the SCR component, and of Pt/Al_2O_3 catalysts with Pt loading ≤ 1% w/w for the PGM component. As an example, Fig. S1 in the Supplementary Information demonstrates the similarity of the NH_3-TPD curves collected over the Cu/CHA component of the present ASC, tested in the form of a single-layer monolith, and over a reference Cu/CHA catalyst (1.7% w/w Cu loading, Si/Al = 6.5) from the literature [41]. To conclusively deconvolve the chemistry of the two system components, dedicated tests were run also over a reference Pt/Al_2O_3 only (single layer) monolith, with a Pt loading close to that of the ASC sample.

2.2. Lab-scale equipment

Passive SCR tests on both the fresh and the aged catalysts were performed over core monolith samples lodged in a sample holder inserted in a stainless-steel tubular reactor (40.5 cm long, 1.5 cm of internal diameter). The reactor was placed in an electric oven, whose temperature was controlled by a PID controller (Eurotherm 2132). In addition, to avoid possible feed bypass, the catalyst was enveloped in a quartz wool ribbon. Three different thermocouples monitored the inlet feed gas, the top and the bottom temperatures of the tested samples.

The feed composition consisted of NH_3, NO, N_2 and O_2, taken from dedicated cylinders. Each feed line was equipped with mass flow controllers (Brooks instrument), filters and one-way valves·H_2O feed was provided by a peristaltic piston pump (Gilson, model 305): before being mixed with the other gases, H_2O was vaporized in a heated pipeline, kept at 190 °C.

The reactor outlet was directly connected to an FT-IR spectrometer (Bruker MATRIX MG5), which continuously provided the concentrations of ammonia, NO, NO_2, N_2O, H_2O during the experimental tests.

Table 1
Industrial ASC catalyst, fresh and hydrothermally aged versions.

Labels	Catalyst	SCR layer	PGM layer	Pt loading
ASC_F	Fresh	Cu/CHA	Pt/Al_2O_3	3 $g/dm^3_{Monolith}$
ASC_ag1	Aged at 750 °C	Cu/CHA	Pt/Al_2O_3	3 $g/dm^3_{Monolith}$
ASC_ag2	Aged at 850 °C	Cu/CHA	Pt/Al_2O_3	3 $g/dm^3_{Monolith}$

2.3. Experimental procedures

Before the activity tests, catalysts were pre-conditioned, by performing a temperature ramp from 150 °C up to 550 °C, with constant heating rate of 15 °C/min, in 5% H_2O and 8% O_2 in N_2 (GHSV = 60000 h^{-1}) and then holding the maximum temperature for 6 h.

Then, dedicated experimental runs were performed, simulating, as much as possible, the rich-lean cycling operating conditions of the Passive SCR converter implemented in the NGVs after-treatment train, placed downstream the TWC. The sequential and periodic shifting between rich (no oxygen in the gas fed, effective NO_X consumption and potential production of ammonia on the TWC) and lean (excess of O_2, lower NO converted on the TWC) engine combustion exhaust gases was simulated in our experimental rig by exposing the tested catalysts alternatively to ammonia (500 ppm ammonia in N_2) and NO+O_2 (500 ppm NO and 8% O_2 in N_2). Feed concentration pulses were kept for 15 min each: although these conditions do not accurately represent the realistic rich-lean cycling frequency of stoichiometric natural gas engines, we aimed herein to collect the complete dynamics of the catalyst in order to fully characterize the related mechanism and calibrate efficiently a transient kinetic model. These tests were run both at low (150 °C) and high (500 °C) temperature; furthermore, at high temperature, similar pulses tests were carried out feeding only O_2 during the lean phase (no NO), in order to better clarify the selectivity of the ammonia oxidation process. Fig. 1 shows the experimental protocol of the low temperature tests, characterized by four series of rich and lean pulses; a similar procedure was adopted during the high-T tests, varying only catalyst temperature.

2.4. Mathematical model

Data collected were analysed by a kinetic model of the ASC catalyst, already developed and successfully used in previous work at Politecnico di Milano. The kinetic schemes describing the activity of the SCR [42] and PGM [19] components of the dual layer system tested were incorporated in a heterogeneous, dynamic, 1D+1D mathematical model of the honeycomb monolith. In the case of the external SCR layer, to ensure a realistic description of the catalytic process, the model considers both external (gas-solid interface) and internal (intra-porous) mass transfer limitations. Regarding the inner Pt-based catalyst, considering its extremely high reactivity, we assumed that only its external surface was effectively active [29]. Thus, the PGM catalyst kinetics was referred to the catalyst geometrical surface area, and directly included in the ASC monolith model. The kinetic parameters of the model were evaluated by a trial-and-error process comparing the simulations with the experimental data collected. The same modelling approach was successfully adopted in past works by some of us [19,27] and by others [28,34] for the modelling analysis of NH_3-SCR experiments performed over dual-layer (SCR + PGM) ASC catalysts.

3. Results and discussion

3.1. Fresh catalyst: low temperature

Fig. 2 shows the experimental data collected over the ASC_F sample under the rich-lean pulses test performed at 150 °C in terms of NO, NO_2, NH_3, and N_2O concentrations with time (symbols).

Starting with the first rich pulse, we observe that NH_3 concentration detected at the reactor outlet slowly increased for the first half of the pulse up to about 50 ppm, showing a significant depletion from the gas phase; then, its dynamic speeded up tending to the feed amount, reaching about 470 ppm at the end of the rich pulse (after 15 min). After closing the NH_3 feed, its concentration rapidly decreased to zero. No traces of NO, NO_2 or N_2O were detected during this transient.

As regards to the subsequent lean pulse (NO+O_2 feed, no ammonia injection), the reactor outlet NO concentration quickly increased right

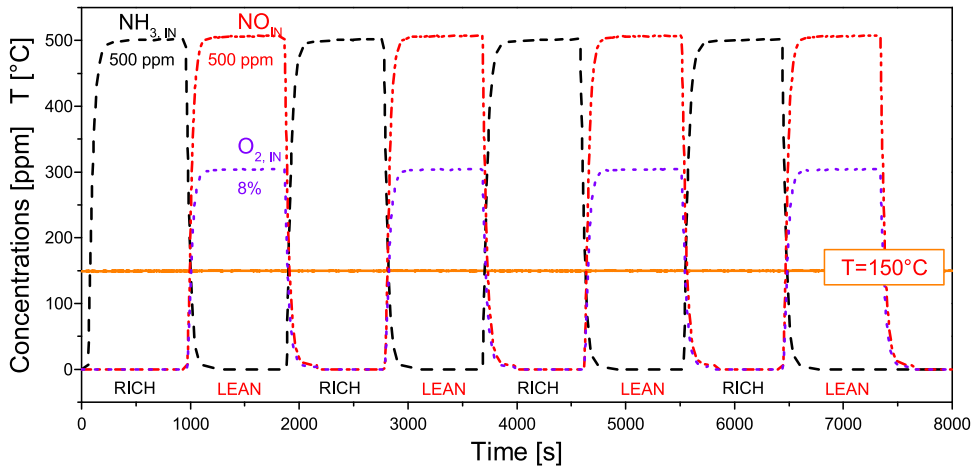

Fig. 1. Experimental protocol of the rich-lean pulses test at low temperature (150 °C): NH_3, NO, and O_2 concentrations of the fed mixture over time. Rich pulses: 500 ppm NH_3, 5% H_2O in N_2; lean pulses: 500 ppm NO, 8% O_2, 5% H_2O in N_2; GHSV= 60000 h^{-1}.

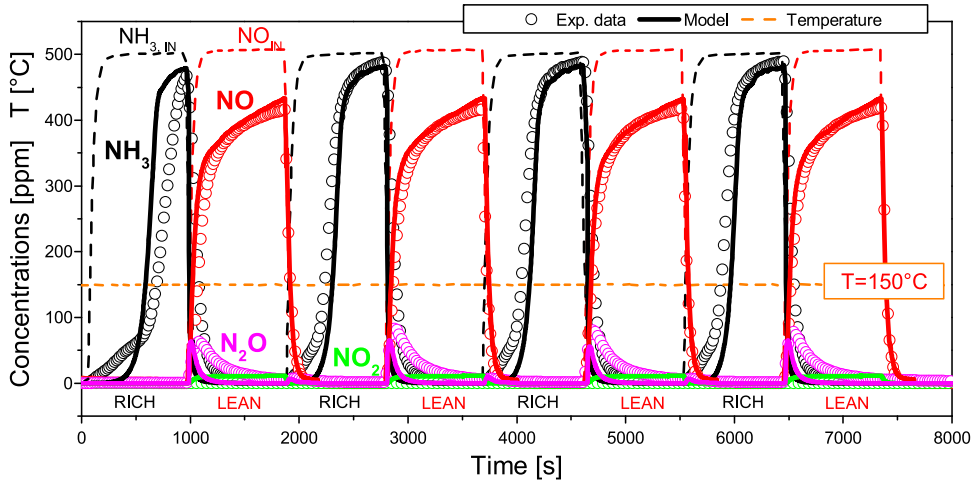

Fig. 2. Rich-lean pulses test at low temperature (150 °C) performed over the ASC_F sample: NH_3, NO, NO_2 and N_2O concentrations detected at the reactor outlet over time. Rich pulses: 500 ppm NH_3, 5% H_2O in N_2; lean pulses: 500 ppm NO, 8% O_2, 5% H_2O in N_2; GHSV= 60000 h^{-1}. Symbols: experimental data; solid lines: model simulations.

after its feed and then slowed down until it reached its maximum at the end of the pulse (about 410 ppm). This dynamic represents the NO conversion during the lean phase, possibly due to Standard SCR reactions occurrence with the ammonia stored during the previous rich pulse. Regarding the selectivity of the NO conversion process, only traces of NO_2 were produced while a significant amount of N_2O was detected: N_2O concentration immediately reached the maximum value right after the NO feed, and then gradually dropped to zero. NO, NO_2, N_2O concentrations decreased to zero when the lean feed stopped.

The dynamics of reactants and products were similarly replicated during the next rich and lean pulses: to better understand the behavior of the fresh catalyst during the oscillating experimental conditions, we isolated the rich phases from the lean phases and analysed separately the performed four pulses by comparing the dynamics of reactants and products concentrations. The comparison is shown in Fig. 3, in terms of NH_3, NO, NO_2 and N_2O concentration trends during both the rich (top graphs) and lean phases (bottom pictures).

From the collected data, aside from the first pulse (Fig. 3, small gray symbols), it was immediately clear that the second, third and fourth pulses resulted almost overlapped (respectively, empty squares, circles and triangles in the graphs of Fig. 3), both considering ammonia concentration during the rich phases and NO consumption and N_2O production during the lean phases. This proves that the activity of the catalyst was stable during the feed composition transients of the performed experimental tests. At low temperatures, as widely demonstrated by the scientific literature on the topic, ammonia was adsorbed and stored (reaction R9) on the SCR layer Cu zeolite catalyst [36,43,44]; then, once NO and oxygen were fed to the reactor during the subsequent lean pulse, the occurrence of the NH_3-DeNOx activity of the SCR catalyst led to the consumption of NO and stored NH_3 selectively to nitrogen, in line with the stoichiometry of the standard SCR reaction reported in reaction R10, or to the undesired production of N_2O, according to the following stoichiometry [43]:

$$NH_3^* + NO + \frac{3}{4}O_2 \rightarrow N_2O + \frac{3}{2}H_2O \quad \text{(R13)}$$

It is important to notice that the dynamics of the NO conversion during the lean phases, although strictly limited by the amount of ammonia available stored during the rich phases, could be affected by the oxygen feed concentration: increasing the oxygen content in the feed gas mixture will result in improving the rate of the standard SCR reaction and, thus, in accelerating the dynamics of NO consumption, and vice versa. However, it is known from the literature that the DeNOx activity of Cu-based SCR catalysts [45] is only slightly affected by the oxygen concentration for O_2 feed contents higher than 1–2%; thus, we assumed that our experimental conditions can represent with

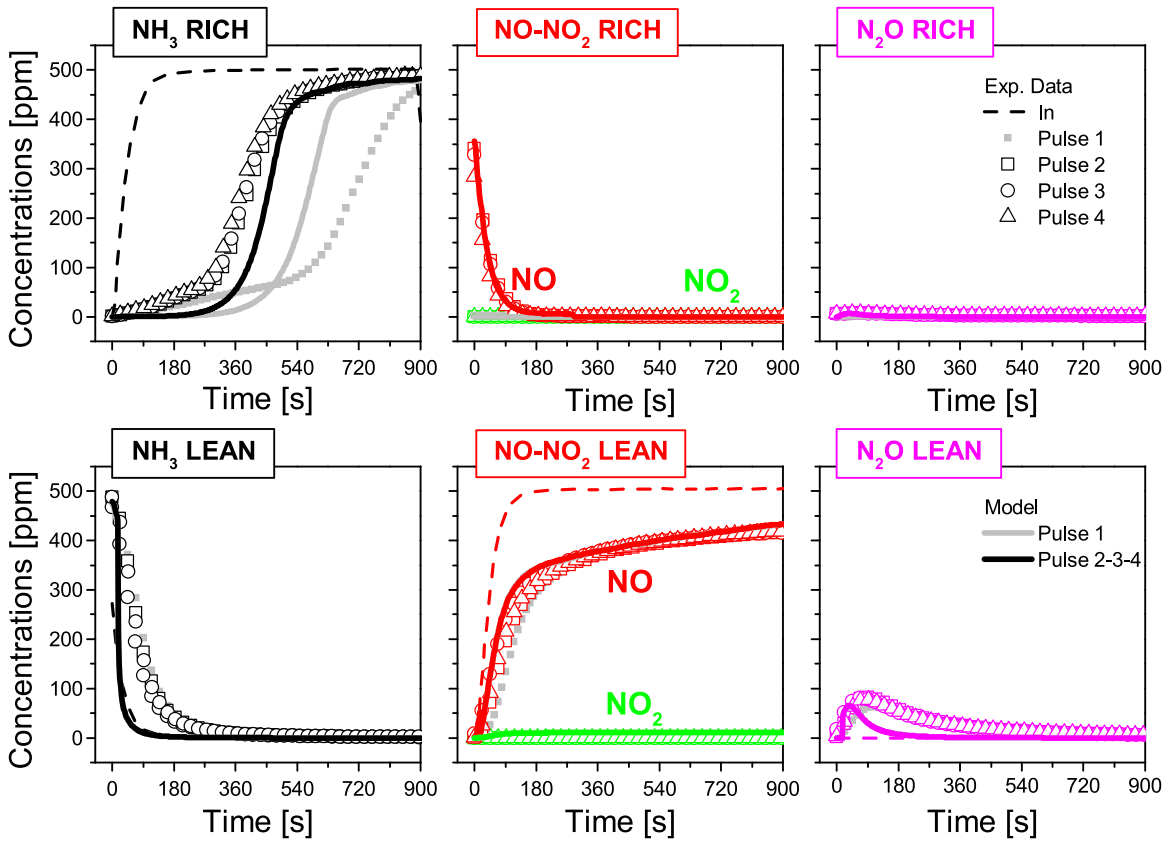

Fig. 3. Comparison between NH_3, NO, NO_2 and N_2O concentrations detected at the reactor outlet during the four rich and lean pulses performed at low temperature (150 °C) over the ASC_F sample. Rich pulses: 500 ppm NH_3, 5% H_2O in N_2; lean pulses: 500 ppm NO, 8% O_2, 5% H_2O in N_2; GHSV= 60000 h^{-1}. Symbols: experimental data; solid lines: model simulations.

satisfactory accuracy the operating regimes of, for example, WHTC cycles performed on natural gas engines [23] (O_2 in the gas feed to the after-treatment system switching from almost 0–20%).

Significant N_2O production under NH_3-SCR operating conditions is typical of noble metal-based and dual-layer ASC catalysts: Colombo et al. [27] reported N_2O yields of about 60% reached during standard-SCR steady-state tests on both a PGM-only system and a double-bed SCR+PGM combined system. At this stage of the work, it is possible to hypothesize that the selective standard SCR reaction to nitrogen proceeds on the SCR layer, while the production of N_2O mostly occurs on the highly active but unselective Pt-based PGM layer. This is in line with the literature [46]: under NH_3-SCR conditions, N_2O formation on Cu-zeolites is reported to be very limited, in the range of 3–10 ppm. On the contrary, as shown by Figs. 2 and 3, our experimental campaign on Cu-zeolite + Pt/Al_2O_3 dual-layer catalysts showed peaks of N_2O production close to 60–70 ppm at low temperature under lean conditions. This is in more consistent with data reported in literature for noble metal-based catalysts [19], such as the PGM component of our dual-layer systems.

To better clarify the ASC activity mechanism at low temperature, the amount of ammonia and NO converted during the rich and lean pulses, respectively, and the amount of N_2O formed during the lean phases were calculated by integrating the concentration traces over time (reactants converted were evaluated from the difference between the integrals of inlet and outlet concentration traces). The computed values are reported in Table 2 for each species and for the different pulses.

Integral values in Table 2 confirm that, apart from the first rich phase, reactants consumption and products formation were consistent during each pulse: at 150 °C, NH_3 is adsorbed on the SCR layer (it is well known in literature that Pt-based PGM catalysts show much lower ammonia storage capacity than Cu-exchanged zeolites [27,40]), and is

Table 2
Low-T test, NH_3 and NO consumption, respectively during the rich and lean pulses; NO_2 and N_2O production during the lean pulses. Values in mmol/$dm^3_{MONOLITH}$.

Pulse	Consumed NH_3 Rich pulse	Consumed NO Lean pulse	Produced NO_2 Lean pulse	Produced N_2O Lean pulse
1	195	78	–	14
2	106	78	–	17
3	104	77	–	16
4	103	76	–	16

subsequently consumed by NO during the lean phases; then, NH_3 storage is refilled during the rich pulses. Indeed, the first ammonia pulse resulted to be different because at the beginning of the experiment no ammonia was stored on the catalyst, leading to a higher consumption of the ammonia fed to the system. At this low temperature (150 °C), because of the low catalyst activity, only part of the ammonia stored during the first rich pulse is consumed during the NO+O_2 feed and, thus, a lower NH_3 amount is needed to restore the storage during the next rich pulse. However, despite the 1:1 consumption ratio involved in the stoichiometries of the reactions R10 and R13, the ammonia depleted from the gas phase and the NO consumption were not equivalent: considering that no traces of other species were detected during the test, this suggests the occurrence of direct ammonia oxidation, possibly over the PGM layer catalyst (reactions R11 and R12).

To confirm this reaction pathway, the same rich-lean cycling at 150 °C was performed over a reference Pt/Al_2O_3 only (single layer) monolith, with Pt loading close to that of the ASC sample: results are reported in Fig. S2 of the supplementary material and in Table S1 as ammonia and NO consumed (and NO_2 and N_2O produced) respectively

during the rich and lean phases. During the rich phases, a limited consumption of ammonia was detected, with outlet concentration almost immediately approaching the feed gas composition. This is due to the weak ammonia storage capacity of this material, in agreement with the proposed reaction mechanism for the dual-layer system: at low temperatures, due to poor activity of the Pt-based layer, only a fraction of the ammonia consumption is related to ammonia oxidation while the main part is due to ammonia storage on the Cu-zeolite component. Furthermore, this results in a low amount of ammonia available during the lean phases, when NO and oxygen are fed to the reactor: accordingly, the experimental data collected showed an almost negligible NO consumption and N_2O production. This also suggests that, in line with the stoichiometry proposed, the N_2O production over the ASC fresh sample requires: i) ammonia stored over the Cu zeolite component; ii) NO and O_2 fed during the lean phases and, iii) a selective PGM component.

As a final comment, the possible effect of other components of the gas stream (such as H_2, CO and unburnt methane) on the ammonia abatement was not included in this study. Nevertheless, at least at low temperatures, an almost negligible effect can be expected on the ammonia storage process. Regarding the DeNOx efficiency during the lean phases, literature studies reported a weak effect of CH_4 on the NH_3-SCR activity of small pore Cu-exchanged zeolites [47,48].

Summarizing, the experimental data collected confirmed the high NH_3 abatement activity of the commercial ASC dual-layer catalyst tested at low temperatures: the wide storage capacity of the SCR catalyst ensures significant ammonia depletion from the gas phase (Fig. 3 shows almost complete consumption of ammonia for about 240 s during every rich pulse) under Passive SCR experimental conditions. It is important to note that the experimental results were obtained shutting down completely the O_2 feed during the rich phases, although this does not correspond to realistic engine operating conditions in which a small fraction of oxygen is always present in the gas mixture. Nevertheless, the ammonia adsorption storage capacity of the SCR component in the dual-layer ASC catalyst structure is not severely impacted by the oxygen content in the gas stream at cold-start temperatures and, thus, its presence in the gas phase will not affect the ammonia abatement performance under these conditions.

3.2. Fresh catalyst: high temperature

The effect of the reactor temperature on the ASC ammonia/NO_X abatement performance was investigated by performing a similar test at higher temperature (500 °C). Results collected are shown in Fig. 4 in terms of NO, NO_2, NH_3, and N_2O concentrations with time (symbols).

Starting from the first rich pulse, ammonia concentration detected at the reactor outlet showed a slightly different dynamics from the low-T data: ammonia was completely consumed for about 60 s; then, its concentration, quickly increased till reaching an almost stationary value at the end of the pulse (about 470 ppm). Once cut off from the feed, the ammonia measured at the reactor outlet dropped to zero, while NO concentration immediately increased to a stationary value (about 410 ppm), and then kept constant during the whole lean pulse. Simultaneously, equimolar NO_2 production was detected (90 ppm), confirming the occurrence of NO oxidation (stoichiometry reported in reaction R14).

$$NO + \frac{1}{2}O_2 \rightleftarrows NO_2 \quad \text{(R14)}$$

Analogous NH_3 and NO_X consumption and NO_2 formation dynamics were observed during the following pulses; however, differently from the low-T test, at high temperature an increase of the ammonia abatement was detected from the first to the other rich phases (maximum NH_3 concentration of about 450 ppm, compared to the 470 ppm of the first pulse). Only small traces of N_2O were produced at high temperature. Fig. 5 show the comparison between the different rich and lean pulses, in terms of ammonia, NO, NO_2 and N_2O concentration dynamics over time.

As in the case of the low temperature, apart from the first rich and lean phases, the catalyst activity was stable during the whole test, replicating the dynamics of reactants consumption and products formations during the second, third and fourth pulses.

Starting from the NO+O_2 feed pulses, the equimolar NO consumption and NO_2 production confirmed the occurrence of NO oxidation only; no traces of NH_3-SCR activity was detected. This is due to the fact that at 500 °C no ammonia adsorption was expected during the rich pulses and, thus, ammonia is not available during the lean phases to trigger the DeNOx reactivity. Nevertheless, significant ammonia consumption was highlighted during every rich pulse, despite the fact that no oxygen nor NO_X were provided. This suggested the occurrence of ammonia oxidation reactions following a redox-type mechanism: ammonia was consumed by means of the oxidized catalytic sites, which were simultaneously reduced. The oxidation state of the catalyst was restored during the lean phases, with the re-oxidation of the catalytic sites by the O_2 fed to the system.

Of course, redox-type mechanisms are not new in literature: in the last years, several efforts have been made to unravel the low-temperature SCR-DeNOx reaction scheme of Cu/zeolite catalysts. While it is widely accepted that the selective reduction of NO_X by ammonia to N_2 and H_2O involves reduction/oxidation half-cycles of the

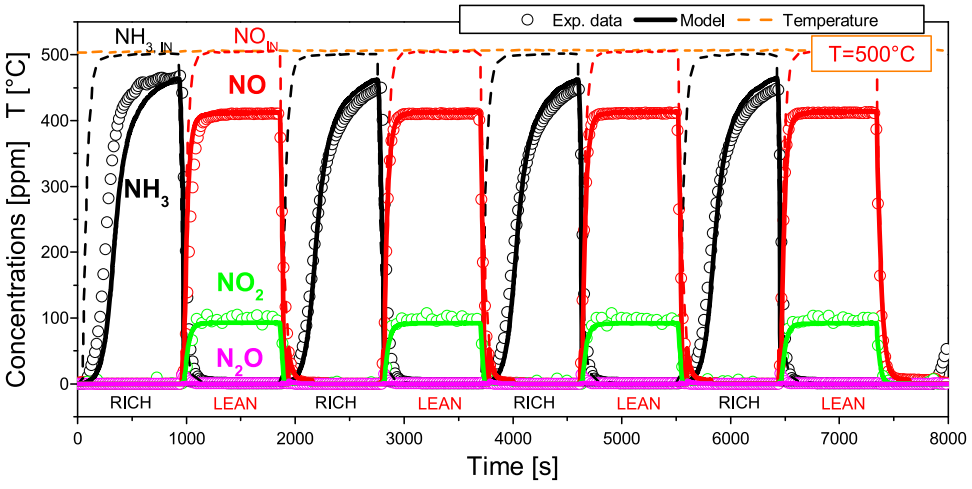

Fig. 4. Rich-lean pulses test at high temperature (500 °C) performed over the ASC_F sample: NH_3, NO, NO_2 and N_2O concentrations detected at the reactor outlet over time. Rich pulses: 500 ppm NH_3, 5% H_2O in N_2; lean pulses: 500 ppm NO, 8% O_2, 5% H_2O in N_2; GHSV= 60000 h^{-1}. Symbols: experimental data; solid lines: model simulations.

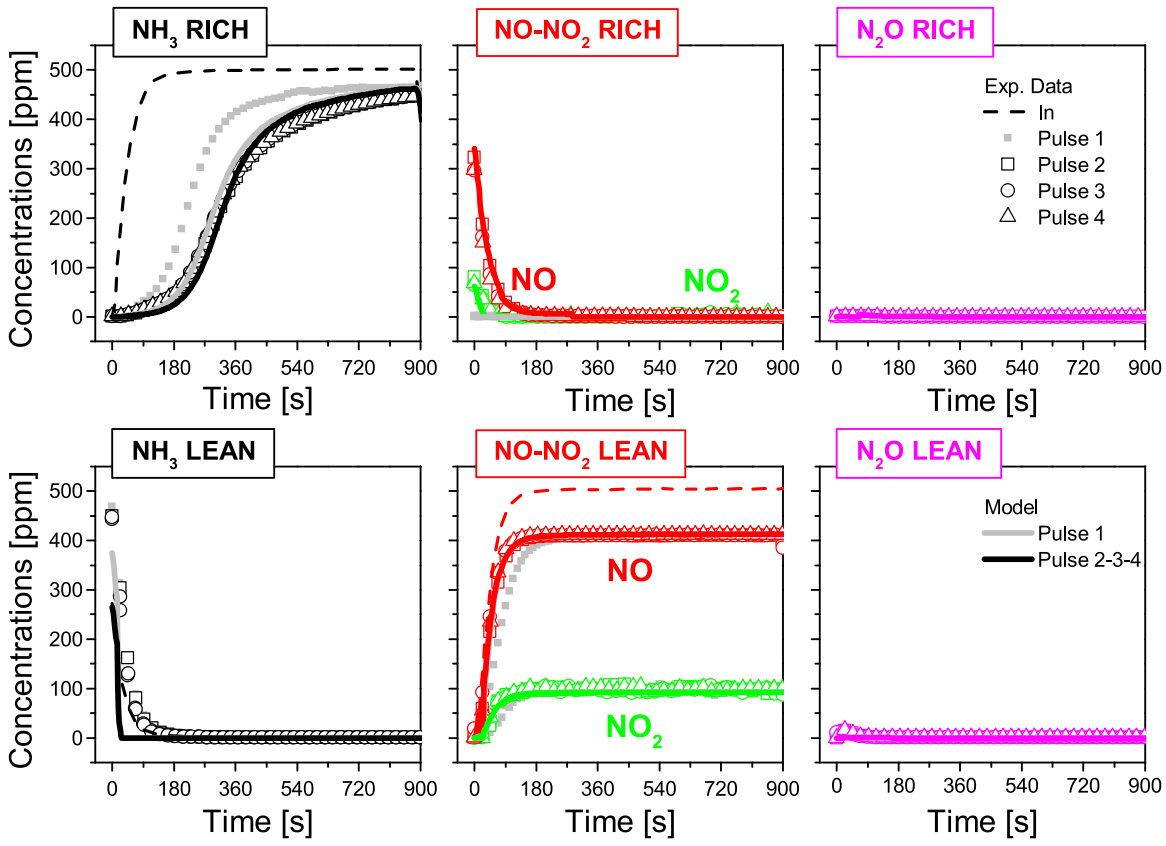

Fig. 5. Comparison between NH_3, NO, NO_2 and N_2O concentrations detected at the reactor outlet during the four rich and lean pulses performed at high temperature (500 °C) over the ASC_F sample. Rich pulses: 500 ppm NH_3, 5% H_2O in N_2; lean pulses: 500 ppm NO, 8% O_2, 5% H_2O in N_2; GHSV= 60000 h^{-1}. Symbols: experimental data; solid lines: model simulations.

Cu active sites, the exact reaction mechanism is still under debate [37,38,49,50]. Recently, through kinetic analysis of transient experiments performed over several commercial Cu/CHA catalysts, we proposed a second order kinetic dependence on the oxidized Cu fraction of the reduction half-cycle rate [36,39,51], demonstrating a dual-site mechanism for the reduction part of the Cu sites redox cycle.

Regarding the Pt/Al_2O_3 catalyst, recent works published by Ghosh et al. [40,52] and Dhillon et al. [35] reported a mechanism that involves both ammonia and oxygen adsorption on the catalytic Pt sites that further interacts to complete the NH_3 oxidation scheme. These results are in good agreement with the experimental data collected herein reported and support our hypothesis of a reaction mechanism that involves firstly the oxidation of the catalytic sites and then their reduction with related NH_3 abatement.

As in the case of the low-T test (Section 3.1), by integrating the concentration dynamics it was possible to evaluate both ammonia and NO consumption and NO_2 formation during our experimental test: calculated values are listed in Table 3.

The first rich pulse highlighted a lower ammonia consumption if compared to the subsequent ones (98 mmol/dm^3_{MON} vs 122 mmol/dm^3_{MON}, as reported in Table 3), probably due to a lower oxidation level of the catalytic sites: no O_2 pre-treatment of the catalyst was performed before the reactive pulses and, thus, the oxidation state of the catalytic sites at the beginning of the test was unknown. Differently from the first, during the other pulses we hypothesized that the oxygen fed during the previous lean phases ensured an almost complete oxidized catalyst leading to a higher ammonia oxidation activity. Thus, ammonia abatement is related to the oxidation state of the catalyst: the higher the amount of oxidized catalytic sites available, the higher the consumption of ammonia, and vice versa.

Table 3 –
High-T test, NH_3 and NO consumption, respectively during the rich and lean pulses; NO_2 and N_2O production during the lean pulses. Values in mmol/$dm^3_{MONOLITH}$.

Pulse	Consumed NH_3 Rich pulse	Consumed NO Lean pulse	Produced NO_2 Lean pulse	Produced N_2O Lean pulse
1	98	55	49	< 1
2	122	49	50	< 1
3	123	50	50	< 1
4	122	49	51	1

Furthermore, although the poor selectivity to nitrogen of the Pt-based PGM catalyst (well documented in literature [27,52]), the absence of by-products formation during the rich pulses (no NO_X nor N_2O, as shown in Fig. 5) demonstrated an almost complete selectivity to nitrogen of the NH_3 oxidation activity under these conditions (high temperature, realistic rich-lean feed composition dynamics). This highlighted the effectiveness of the dual-layer configuration: unselective ammonia oxidation products from the inner PGM layer are efficiently converted to nitrogen by the selective NH_3-SCR activity of the Cu-zeolite external layer. These results were also confirmed by the tests at high temperature performed over the reference single-layer Pt/Al_2O_3 only catalyst, reported in Fig. S3 and Table S2 of the revised manuscript. During the rich phases, ammonia was efficiently converted by direct oxidation, reducing the Pt sites; again, catalytic activity was then restored by the oxygen fed during the lean phases.

To validate the mechanism proposed, we performed an additional test, repeating the series of pulses at high temperature (500 °C) in the absence of the NO feed during the lean feed, when only oxygen was flowing into the reactor. The collected results are shown in Fig. 6 in terms of NO, NO_2, NH_3, and N_2O concentrations with time (symbols).

As expected, ammonia concentration dynamics were very similar to

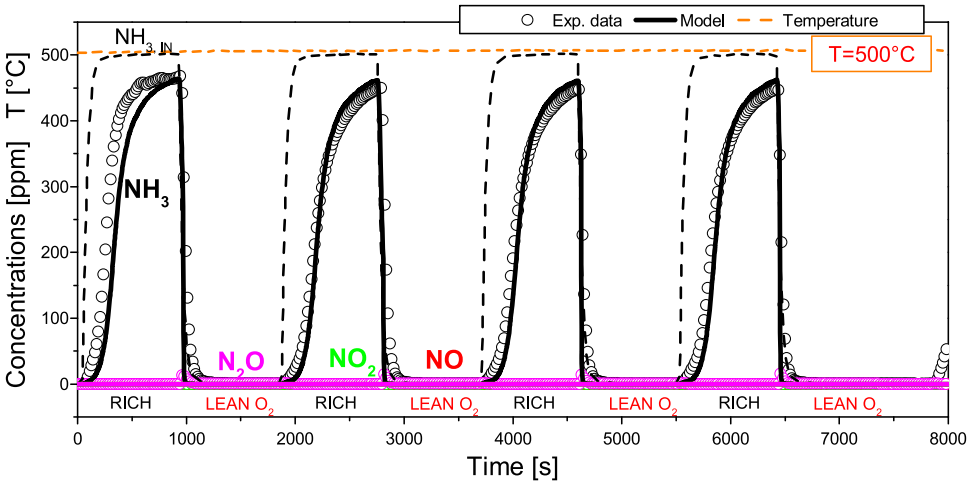

Fig. 6. Rich-lean (no NO) pulses test at high temperature (500 °C) performed over the ASC_F sample: NH_3, NO, NO_2 and N_2O concentrations detected at the reactor outlet over time. Rich pulses: 500 ppm NH_3, 5% H_2O in N_2; lean pulses: 8% O_2, 5% H_2O in N_2; GHSV= 60000 h^{-1}. Symbols: experimental data; solid lines: model simulations.

those observed during the test performed in the presence of NO during the lean phases (Fig. 4): data showed an important deadtime before breakthrough at the reactor outlet (almost 3 min during the second, third and fourth rich pulses), then NH_3 concentration progressively increased, reaching its maximum value (about 450 ppm) at the end of the pulse. By integrating the dynamics of the NH_3 concentration, it was found that the NH_3 converted was equivalent to the case of the test performed with NO (Table 3); furthermore, as in the previous test, no traces of unselective products were detected during the whole test despite the significant ammonia oxidation activity.

These data confirmed the redox nature of the ammonia oxidation mechanism over the tested catalyst, and, in particulars, over the PGM layer: Pt sites are oxidized by oxygen during the lean phases and reduced by ammonia during the rich phases, leading to NH_3 conversion. The abatement efficiency gradually decreased during the NH_3 feed due to the progressive reduction of the Pt sites available. The overall selectivity to nitrogen was ensured by the activity of the SCR layer on top of the PGM: oxidized Cu sites efficiently converted to nitrogen the unselective products of the Pt-based catalyst that were back-diffusing through the SCR layer, taking part into the redox cycles themselves. As the platinum, Cu sites were re-oxidized by the oxygen fed during the lean phases.

This mechanism explains also the discrepancy between NH_3 and NO consumption reported during the low-temperature test (Table 2, Section 3.1 of this work): besides the NH_3 adsorption and further consumption by the NO fed during the lean pulses, part of the ammonia fed was directly converted by the occurrence of ammonia oxidation, even at 150 °C, under transient experimental conditions.

However, the experimental tests reported demonstrated the capacity of the fresh sample tested to efficiently convert the fed ammonia under passive SCR conditions, also at high temperature: the oxidation state of the catalyst (ensured by the oxygen present in the exhaust gases during the lean engine combustion conditions over the full-scale converters) appeared to play a key role in NH_3 abatement performance of passive SCR after-treatment step. As in the case of low-T conditions, the complete absence of O_2 in the fed mixture should not significantly affect the mechanistic conclusions: the presence of sub-stoichiometric oxygen during the rich phases under realistic engine operating conditions will results in increasing the oxidative state of the catalyst and, thus, the overall abatement of ammonia by means of the redox catalytic process.

Finally, as in the case of the low-T tests, it is important to report that the effect on ammonia abatement of H_2, CO and unburned methane was not studied at this stage of the work; in particular, a significant competition between hydrogen and ammonia can occur in the oxidation over the catalytic sites. This effect will be investigated in future work.

3.3. Mathematical model of NH_3 abatement

The experimental data shown in Sections 3.1 and 3.2 of this work demonstrated the occurrence of two different NH_3 abatement mechanisms over ASC catalysts exposed to realistic transient passive SCR operating conditions: at low temperatures, ammonia produced by the upstream TWC catalyst under rich combustion conditions can be efficiently stored on the SCR layer of the ASC, and then further consumed by NO_X and oxygen via the NH_3-SCR process. On the other hand, when the after-treatment system temperature is high enough to ensure satisfactory catalytic activity, ammonia is directly converted by direct oxidation by the Pt sites of the PGM layer, following a redox mechanism. Surprisingly, this process was found to be almost completely selective to nitrogen, even at very high temperatures.

Consequently, we developed a reaction mechanism that includes two simultaneous redox cycles, both for Pt sites in the PGM layer and for the Cu sites in the SCR layer. The list of reactions included in the kinetic scheme is reported in Table 4, together with the corresponding rate equations and parameter estimates.

In the SCR layer, the NH_3 adsorption/desorption mechanism on a lumped storage S_1 site is described by reactions R15 and R16, with well-established rate expressions taken from the SCR literature, including non-activated NH_3 adsorption as well as a coverage dependent NH_3 desorption energy [19,32,36,43,44]. The consumption of the stored ammonia (NH_3*) by NO_X according to the standard SCR reaction, with the consequent reduction of the oxidized Cu sites (S_2-O), is described by R17. The associated rate equation is first order in NO and second order in the fraction of oxidized Cu sites, which is consistent with a recent transient kinetic study of the SCR reduction half cycle over Cu-CHA catalysts [36,51]. The SCR model further includes the global NO oxidation reaction R18, to describe the NO_2 production detected during the high temperature tests (Section 3.2, Figs. 4 and 5). The empirical rate equation for R18 accounts both for the thermodynamic equilibrium constraint and for the well-known NO_2 inhibition effect [19,27]. The SCR redox cycle is closed by R19, which represents the reoxidation of the reduced Cu (S_2) by O_2: for this step, a simple empirical rate equation is assumed that is first order both in the oxygen partial pressure and in the fraction of reduced Cu sites.

A similar kinetic mechanism was adopted for the PGM layer, too. The ammonia adsorption/desorption process on lumped S_3 sites is described by reactions R20 and R21 in Table 4. Despite no significant ammonia storage is typically measured over noble metal-based catalysts, adsorption and desorption kinetic steps are often adopted in the literature to model the PGM catalytic performance in ammonia slip catalysts [19,40,

Table 4

Reaction mechanisms, rate expressions [mol/s/$m^3_{monolith}$] and estimated reaction parameters. Rate constants in Arrhenius form: $k_R = A * exp\left(-\frac{E_{Act}}{R*T}\right)$, *EActin kJ/mol.*

Rate constant for R16, Temkin isotherm: $k_{des\ S1} = A * exp\left(-\frac{E_{des\ S1}(1-0.55*\theta_{NH3})}{R*T}\right)$; E_{desS1} in kJ/mol.

SCR LAYER					
Label	**Reaction**	**Stoichiometry**	**Kinetic expression**	**A**	**E_{Act}**
R15	NH_3 Ads	$S_1+NH_3 \rightarrow NH_3*$	$r_{ads\ S1} = k_{ads\ S1}\ C_{NH3}(1-\theta_{NH3})$	7.54 e2	–
R16	NH_3 Des	$NH_3* \rightarrow S_1+NH_3$	$r_{des\ S1} = k_{des\ S1}\theta_{NH3}$	2.60 e10	124.7
R17	Standard SCR	$4NO+4NH_3*+2\ S_2\text{-}O \rightarrow 4\ N_2+6\ H_2O+2S_2$	$r_{SCR} = k_{SCR}\theta_{NH3}\ C_{NO}\theta_{O2}^2$	4.15 e16	124.7
R18	NO Oxidation	$2NO+O_2 \rightarrow 2NO_2$	$r_{NO} = k_{NO}(C_{NO}\sqrt{P_{O2}} - \frac{C_{NO2}}{Keq})\frac{1}{1+K_{NO2}\ C_{NO2}}$	3.02 e4	44.9
R19	SCR Sites Oxidation	$2S_2+O_2 \rightarrow 2S_2\text{-}O$	$r_{ads\ S2} = k_{ads\ S2}\frac{P_{O2}}{0.08}(1-\theta_{O2})$	1.85 e8	–
PGM LAYER					
Label	**Reaction**	**Stoichiometry**	**Kinetic expression**	**A**	**E_{Act}**
R20	NH_3 Ads	$S_3+NH_3 \rightarrow NH_3*$	$r_{ads\ S3} = k_{ads\ S3}C_{NH3}(1-\theta_{NH3}^{PGM})$	8.29 e3	–
R21	NH_3 Des	$NH_3* \rightarrow S_3+NH_3$	$r_{des\ S3} = k_{des\ S3}\theta_{NH3}^{PGM}$	7.16 e16	85.7
R22	NH_3 Oxidation	$2NH_3*+3S_4\text{-}O \rightarrow N_2+3\ H_2O+3S_4$	$r_{NH3OX} = k_{NH3OX}\ \theta_{NH3}^{PGM}\theta_{O2}^{PGM\,2}$	2.04 e21	149.7
R23	SCR (N_2O)	$4NO+4NH_3*+6S_4\text{-}O \rightarrow 4\ N_2O+6\ H_2O+6S_4$	$r_{SCR}^{PGM} = k_{SCR}{}^{PGM}\ C_{NO}\ \theta_{NH3}^{PGM}\theta_{O2}^{PGM\,2}$	2.04 e18	83.1
R24	PGM Sites Oxidation	$2S_4+O_2 \rightarrow 2S_4\text{-}O$	$r_{ads\ S4} = k_{ads\ S4}\frac{P_{O2}}{0.08}(1-\theta_{O2}^{PGM})$	1.85 e8	–
R18_B	NO Oxidation	$2NO+O_2 \rightarrow 2NO_2$	$r_{NO} = k_{NO\_PGM}(C_{NO}\sqrt{P_{O2}} - \frac{C_{NO2}}{Keq})\frac{1}{1+K_{NO2}\ C_{NO2}}$	1.58 e5	44.9

52]. For these steps we assume the same rate expressions as for the SCR layer. The stored ammonia is then oxidized to N_2 and to N_2O, simultaneously reducing the Pt sites (S4-O to S4), according to reactions R22 and R23, respectively. For both such Pt reduction steps we again assume second order rate equations in the fraction of oxidized metal sites [28]. Reaction R18_B accounts for the NO_2 production due to direct NO oxidation on the PGM layer (clearly apparent in Fig. S3 and Table S2 of the Supplementary material). The re-oxidation of the catalyst completes the mechanism (reaction R24). For both the R18_B and R24 steps we adopt the same rate expressions of the equivalent steps in the SCR kinetic model, i.e., R18 and R19.

It worth noticing that the oxidation half cycles of the active sites in both the SCR and the PGM layer are schematically represented in our redox model as "oxygen adsorption" steps: an oxygen molecule interacts with a couple of reduced sites (S_2 or S_4) to form oxidized species (S_2-O or S_4-O). Although this is a simplification of the actual redox mechanism, a similar approach has been successfully adopted in the literature to model both DeNOx reduction transients of SCR Cu/zeolites [36], and the NH_3 oxidation activity of Pt/Al_2O_3 commercial catalysts [40,52].

The proposed kinetic scheme was then incorporated in the mathematical model of dual-layer ASC monolith catalyst developed by Colombo et al. [27], which takes into account also external and intra-porous mass transfer limitations across the SCR layer, while assuming the inner PGM layer as an active catalytic surface (due to its extremely high activity).

The calibration of the rate parameters (pre-exponential factor and activation energy of an Arrhenius-type rate constants k_R for the reactions in Table 4) was performed by trial-and-error, comparing the simulated outlet concentration traces of NO, NO_2, N_2O and NH_3 with the experimental results. Notably, since it was not possible to monitor the consumption of oxygen during the experimental campaign with the FT-IR analyzer, the oxidation part of the redox cycles could not be accurately calibrated. The rate constants for steps R19 and R24 were roughly estimated by simply assuring that all the Cu and Pt sites were fully oxidized by the oxygen fed during the lean pulses, and no attempt was made to assess their temperature dependence.

The best estimates of the rate parameters are appended to Table 4, with units corresponding to reaction rates expressed in mol/s per unit volume (m^3) of monolith catalyst. For the SCR layer, the estimates of both the NH_3 desorption energy at zero coverage (R16) and the Standard SCR activation energy (R17) in Table 4 are in line with the parameters of the equivalent SCR reaction steps over Cu-SSZ-13 reported in a recent study of a dual-layer Cu-SSZ-13 + Pt/Al_2O_3 ammonia oxidation catalyst [35]. The NH_3 desorption energy at zero coverage (124.7 kJ/mol) is also comparable to the corresponding estimate from a recent kinetic modelling study over Cu-SSZ-13 (135 kJ/mol) [44].

For the PGM layer, the fitted NH_3 desorption energy (~86 kJ/mol) is somewhat lower but not too far from the corresponding estimates for Pt-catalysed NH_3 oxidation (e.g., 110 kJ/mol in [35]), while the estimated activation energy of the lumped NH_3 oxidation step R22 (~150 kJ/mol) is remarkably similar to the corresponding estimate from the same source (145 kJ/mol).

The kinetic calibration of the NO oxidation steps R18 (for the SCR layer) and R24 (for the PGM layer) was challenging due to their poor activity in the low temperature regime, and to the dominant role of NO oxidation in the PGM layer in the high temperature regime, governed by chemical equilibrium. Thus, a single estimate of the activation energy was assumed for both reaction steps. A sensitivity analysis showed that the predicted overall performance of the dual-layer system was in fact insensitive to gross variations of the R18 rate.

As shown by the solid lines in Figs. 2 to 6, the calibrated kinetic mechanism was able to accurately describe the concentration dynamics of both reactants and products during the rich-lean transient tests.

At low temperature (150 °c, Figs. 2 and 3), NH_3 adsorption on the SCR layer under rich pulses conditions, combined with its further consumption by standard SCR during the lean phases (or by unselective SCR with N_2O formation over the PGM layer) with reduction of the catalytic sites, played a significant role in the overall ASC catalytic performance. The redox cycle is closed by the re-oxidation of the catalytic sites by the oxygen feed. The model was also able to describe the higher ammonia consumption detected during the first rich pulse if compared to the others: at the beginning of the test, in fact, the SCR sites were empty, enabling higher adsorption from the gas phase. Additionally, assuming that part of the ammonia fed during the rich pulses is directly converted according to an oxidation mechanism due to the oxygen "stored" on the catalytic sites allows to describe the greater ammonia depletion compared to NO consumption highlighted by the integral values reported in Table 2.

At 500 °C (Figs. 4, 5 and 6), NH_3 concentration trends were successfully predicted by the ammonia oxidation mechanism occurring over the PGM layer, with the conversion decrease during the rich pulses nicely matched by the progressive consumption of the oxygen stored

(reduction) on the Pt catalytic sites. The abatement activity was restored by re-filling the Pt sites with oxygen during the lean pulses; concluding, NO_2 production resulted from NO oxidation in the SCR layer.

Finally, to accurately describe the dynamics of the first rich pulse at high temperature, we assumed an initial partial oxidation state of the catalyst, leading to a lower NH_3 abatement performance if compared to the following ones.

It is worth noticing that the reduction steps in the proposed reaction scheme (R17 for the SCR catalyst and R22 and R23 for the PGM layer) incorporate a second order dependence with respect to the oxidized catalytic sites in the kinetic expressions. In the case of the SCR catalyst, this assumption is in line with literature findings [36,51] on the modelling of reduction transients over commercial Cu/zeolite catalysts. Nothing similar was found in literature for the Pt/Al_2O_3 NH_3 oxidation activity; however, by assuming the same kinetic dependence in the reduction for the Pt sites, the accuracy of the model improved in simulating the dynamics of the NH_3 concentration under the experimental conditions investigated.

Concluding, it is important to remark that the model herein developed represents a simplified approach to describe the activity of the dual-layer ammonia slip catalyst tested under transient operating conditions. For example, as reported before, the oxidation of the active sites is simplified as oxygen adsorption elementary steps while their reduction is lumped in the standard SCR and ammonia oxidation global reactions, respectively, for the SCR and PGM components. A more detailed approach should include the whole set of elementary steps of the reaction mechanism; nonetheless, we think that the kinetic scheme of this work provides at least a significant framework to rationalize the NH_3 and NOx abatement mechanisms over dual-layer ammonia slip catalysts. Further developments of the model, beyond the analysis of the oxidation and reduction half-cycles of the redox cycle, may include the extension of the analysis to intermediate temperatures and to different NH_3 and NOx feed compositions, thus covering a wider range of realistic operating conditions.

3.4. *Ageing effect: tests and modelling analysis*

The same experimental campaign performed over the fresh sample (ASC_F) was repeated over two aged version of the ASC catalyst, named ASC_ag1 and ASC_ag2 (Table 1, Section 2.1). These tests were used to study the loss of NH_3 (and NO_X) abatement performance due to the ageing of the catalyst as well as to validate the accuracy of the reaction scheme proposed and reported in Section 3.3.

The experimental results collected over the aged samples (reported in the Supporting Information as Figs. S4, S5, S6 and S7, respectively for low and high temperature tests over samples ASC_ag1 and ASC_ag2) were qualitatively in agreement with the results showed for the fresh catalyst, confirming the mechanism proposed in this work. The same dynamics of ammonia and NO consumptions were observed during the rich and lean pulses as well as the difference from the first with the other pulses. Thus, it is possible to clearly quantify the effect of the ageing process on the catalytic performance by comparing the dynamics of reactants and products during one of the latter rich-lean sequence performed during the tests. Fig. 7 shows, as an example, the comparison of the second pulse run at low temperature (150 °C) over the ASC_F sample, and the two aged: more specifically, NH_3 concentration detected during the second rich phases, and NO and N_2O dynamics collected during the second lean pulses are represented. Indeed, as already observed for the ASC_F sample, both the rich and lean second, third and fourth phases performed over the aged samples resulted almost overlapped, confirming stable catalytic performance: accordingly, in Fig. 7 we included only the second pulses, as representative of the activity of the tested catalysts.

During the rich phase, the ASC_ag1 ammonia concentration profile (circles in Fig. 7) was similar to the ASC_F one (squares), showing a deadtime before NH_3 breakthrough at the reactor outlet and then an

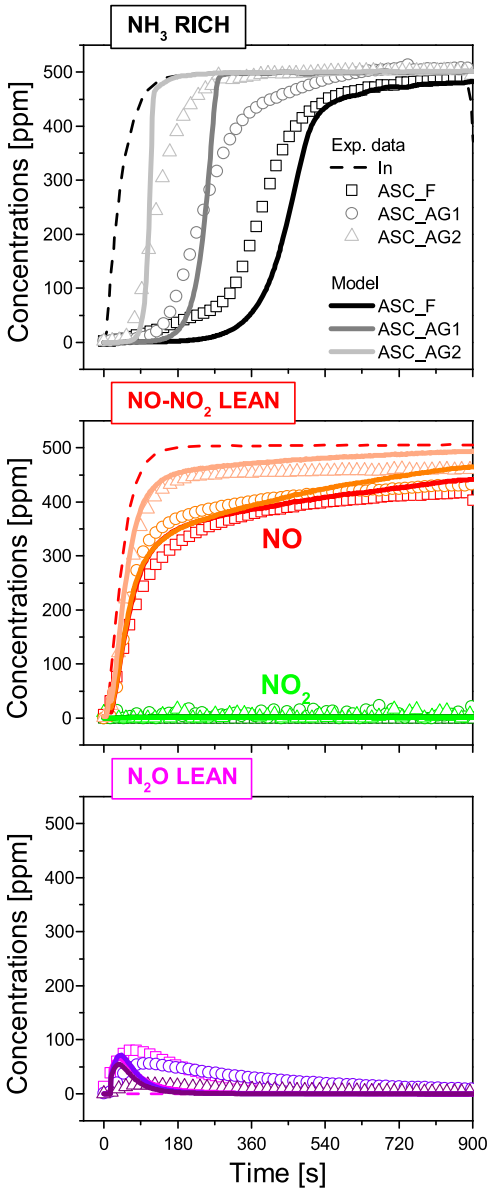

Fig. 7. Low temperature test (150 °C), second rich and lean pulse performed over ASC_F, ASC_ag1 and ASC_ag2 samples: NH_3 concentration during the rich pulses and NO and N_2O during the lean pulses over time. Rich pulses: 500 ppm NH_3, 5% H_2O in N_2; lean pulses: 500 ppm NO, 8% O_2, 5% H_2O in N_2; GHSV= 60000 h^{-1}. Symbols: experimental data; solid lines: model simulations.

increase tending to the inlet feed amount; however, the overall performance was significantly lower, with an early NH_3 release and, thus, a smaller amount depleted from the gas phase. The same effect was even more highlighted over the more severely aged ASC_ag2 sample (triangles in Fig. 7). Nevertheless, it is important to notice that, under these transient conditions, no NH_3 slip was detected for at least 60–70 s over all the tested catalysts. Considering that, under realistic dithering operating conditions, the ammonia concentration peaks detected downstream the ATS (produced by the TWC catalyst) lasted typically few seconds [23], these data suggested that even the most aged sample is theoretically able to effectively convert the ammonia present in the fed gases. Additionally, as in the case of the fresh sample, no NO_X nor N_2O formation was detected during the rich pulses over both the aged samples.

As regards NO abatement during the lean phase, its conversion on the ASC_ag1 sample was slightly decreased compared to ASC_F

performance, while a significant loss was observed over the ASC_ag2 catalyst; while no NO_2 production was detected, some N_2O was formed during the lean pulses for all the catalyst tested, reaching a maximum concentration right after the NO+O_2 feed and then slowly decreasing to zero during the pulse.

Directly comparing the dynamics of the ammonia concentration, or the amount of moles converted, provides an immediate picture of the difference between the catalysts but is not perfectly accurate. To directly compare the activity of the tested samples, we report in Table 5 the calculated amounts of NH_3 and NO converted and N_2O produced, during the rich and lean cycles respectively, obtained by integrating over time the corresponding concentrations.

Differently from the fresh sample, the aged catalysts showed a progressively lower but equimolar consumption of ammonia/NO during the rich/lean pulses; this is in good agreement with the mechanism incorporated in the reaction scheme proposed, with NH_3 adsorption and further conversion by NO+O_2 feed through NH_3-SCR activity. Consequently, it is possible to hypothesize that the ageing process directly affected the NH_3 storage capacity of the SCR layer of the catalyst, decreasing the amount of the NH_3 that can be stored on the catalytic surface. The decrease in the DeNOx activity did not result in a significant N_2O formation reduction, leading also to a decrease in the overall selectivity of the process.

Furthermore, the comparison between the integrated values suggested a loss of the ammonia oxidation activity at low temperature on the ASC_F sample, thus highlighting a decreased activity of the Pt-based PGM layer as a consequence of the ageing process.

This effect was confirmed by the high temperature (500 °C) test: data are shown in Fig. 8, comparing the second rich and lean pulses collected over the fresh (squares) and aged catalysts (ASC_ag1: circles; ASC_ag2: triangles), while integrated values are reported in Table 5.

As reported in Section 3.2 for the fresh sample, ammonia oxidation abatement at 500 °C during the rich phases proceeded by direct ammonia oxidation, mostly over the Pt sites of the PGM layer, through a redox-like reaction mechanism. Data collected over the aged catalysts confirmed this hypothesis: at 500 °C, no stable ammonia storage during the rich and, thus, no NH_3-SCR activity during the lean pulses could be achieved, and NO is equimolarly converted to NO_2 (as reported in Table 5) through NO oxidation. However, lean oxygen feed ensured the oxidation of the catalytic sites (of both SCR and Pt layers), enabling NH_3 oxidation activity during the rich pulses.

Indeed, from the NH_3 concentration dynamics over the aged samples shown in Fig. 8, it is immediately clear the loss of ammonia oxidation activity recorded during the rich pulses at high temperature: no significant deadtime was highlighted, with immediate ammonia release at the reactor outlet right after its feed. Then, outlet NH_3 concentration slowly increased, approaching the feed composition at the end of the pulse. Values of overall ammonia converted reported in Table 5 confirmed this trend, progressively decreasing with increasing ageing conditions, from 120 mmol/dm^3_{MON} in the case of the fresh sample to 74 and 52 mmol/dm^3_{MON}, respectively for the ASC_ag1 and ASC_ag2 samples.

Table 5
Low-T and high-T tests, NH_3 and NO consumption, respectively during the rich and lean pulses; NO_2 and N_2O production during the lean pulses. Values in mmol/$dm^3_{MONOLITH}$.

Catalyst	Consumed NH_3 Rich pulse	Consumed NO Lean pulse	Produced NO_2 Lean pulse	Produced N_2O Lean pulse
Low temperature test (150 °C)				
ASC_F	104	77	–	17
ASC_ag1	58	61	–	16
ASC_ag2	26	30	–	15
High temperature test (500 °C)				
ASC_F	120	49	50	< 1
ASC_ag1	74	33	33	< 1
ASC_ag2	52	24	25	< 1

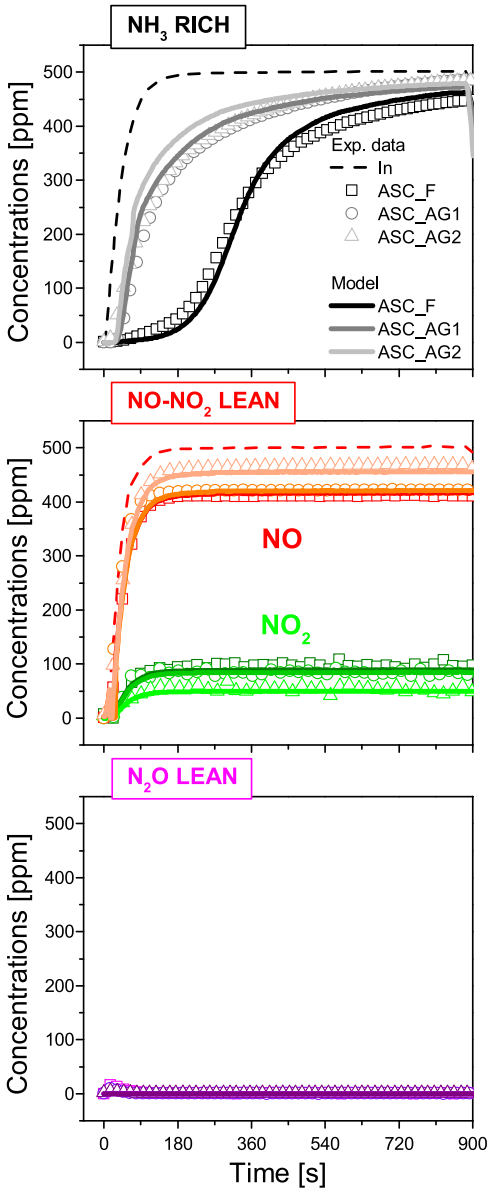

Fig. 8. High temperature test (500 °C), second rich and lean pulse performed over ASC_F, ASC_ag1 and ASC_ag2 samples: NH_3 concentration during the rich pulses and NO and N_2O during the lean pulses over time. Rich pulses: 500 ppm NH_3, 5% H_2O in N_2; lean pulses: 500 ppm NO, 8% O_2, 5% H_2O in N_2; GHSV= 60000 h^{-1}. Symbols: experimental data; solid lines: model simulations.

Surprisingly, the N_2 selectivity of NH_3 oxidation was conserved also over the aged catalysts: no NO_X nor N_2O traces were detected during the rich pulses, suggesting that the SCR layer was still efficiently working. Similar results in terms of ammonia conversion (and selectivity) dynamics were obtained performing the same high temperature test without feeding NO during the lean pulses, as showed in Section 3.2 for the fresh catalyst (results reported in Fig. S8 in the Supporting material), confirming the picture described by the reaction scheme proposed for the fresh system also for the aged catalysts.

Summarizing, the collected data suggest that the decrease in ammonia abatement activity due to the progressive ageing of the commercial ASC catalyst tested in this work can be ascribed both to a decreased NH_3 storage capacity of the SCR layer (that is relevant at low temperatures) and to the loss of overall NH_3 oxidation activity of the Pt sites in the PGM layer (that is critical at high temperatures).

The model developed for the fresh sample was able to efficiently

predict the performance of the two aged samples tested, as well, as shown by the solid curves in Figs. 7 and 8 (and S8 of the Supporting material). Simulations were performed by simply varying the NH_3 storage capacity of the SCR layer (475 mol/$m^3_{active\ phase}$ for the fresh sample, decreased to 300 and 100 mol/$m^3_{active\ phase}$ respectively for the ASC_ag1 and ASC_ag2 samples), without varying the reaction scheme or any other kinetic parameters calibrated for the ASC_F sample. Regarding the kinetics of the PGM layer, a simple multiplicative factor was included in the reaction scheme to describe the decrease of its activity, again without varying the estimated parameters: by comparing the simulations with the experimental data, it was found that the NH_3 oxidation activity was 20 and 25 times lower respectively for the ASC_ag1 and ASC_ag2 samples compared to the fresh catalyst. Possibly, this latter effect is related to the sintering and/or volatilization of the Pt sites of the PGM component in the dual-layer structure, which are the primary sources of deactivation due to ageing of noble metal-based catalysts [53–55]. As a final remark, it is important to note that, according to our modelling analysis, the PGM Pt-based catalyst was more severely affected by the ageing process compared to the SCR component of the dual-layer systems investigated.

Since the model was fitted manually to the data, no statistical analysis of the rate parameter estimates is available. However, the proposed model was able to describe with good accuracy the transients of reactants and products concentrations during runs at different temperatures (150–550 °C), with different protocols (with and without NO in the feed) and over different catalysts (fresh and two aged versions). We believe that this represents an effective (though not formal) validation of the model adequacy.

Even if we have used a simple approach to describe a complicated catalytic system, we would like to point out the significance of the modelling analysis performed on transient experimental data and the importance of the conclusions reached with the present work, both for the elucidation of the NH_3 abatement mechanisms in different temperature regimes and for the assessment of the ageing effect on the ASC catalytic activity.

4. Conclusions

This work was focused on the experimental and modelling study of the NH_3 abatement performances of commercial ASC catalysts under passive SCR conditions. A set of tests were performed to study the activity of a fresh and two progressively aged samples under feed composition transients, replicating the full-scale operating conditions of a catalytic device placed downstream of a TWC in NGVs after-treatment systems. Rich combustion and consequent ammonia formation over the TWC were simulated by 500 ppm NH_3 feed pulses in the absence of oxygen; the switch to lean combustion was simulated by instantaneously varying the feed composition, cutting off the NH_3 feed and injecting NO and O_2. To extensively study the catalytic performance, the tested sample was exposed to several feed concentration transients, at both low (150 °C) and high temperature (500 °C).

At low temperature, data collected over the fresh sample showed that ammonia is adsorbed on the SCR catalyst layer during the rich pulses and then further consumed, mostly via NH_3-SCR reactions, during the lean pulses. Differently, at high temperatures ammonia is directly converted by NH_3 oxidation through a “redox” mechanism involving oxygen storage on the catalytic sites and its further consumption (reproducing the oxidation/reduction cycle); during the lean pulses, the oxygen feed enables the re-oxidation of the active sites, restoring the catalytic activity. NO consumption during the lean phases suggests that no ammonia adsorption was occurring at 500 °C; furthermore, despite NH_3 oxidation over Pt-based catalysts, complete N_2 selectivity is ensured during the feed composition transients by the SCR layer. The predictive model developed from this simple reaction scheme can accurately predict the dynamics of reactants consumption and products formation both at low and at high temperature.

At low temperature, the catalyst ageing results primarily in a significant loss of ammonia storage capacity; nevertheless, complete ammonia abatement is still attainable for about 60–70 s after its feed. On the contrary, at high temperature the ammonia oxidation activity is strongly affected by the catalyst ageing, dramatically decreasing both the overall conversion and the consumption dynamics. Surprisingly, even in the case of the aged catalysts, the ammonia oxidation selectivity to N_2 is complete. Varying neither the reaction scheme, nor the kinetic parameters calibrated on the fresh sample, the model can accurately describe the experimental data collected over the aged samples by simply adjusting the ammonia storage capacity of the SCR layer and an overall activity factor for the PGM catalyst layer.

To our knowledge, a modelling analysis that incorporates the redox features of NH_3-SCR DeNOx catalysts applied to the control of ammonia slip from NGVs is a novelty in the scientific literature. On one side, by this modelling approach we have demonstrated and rationalized that inclusion of a dedicated ammonia abatement catalytic step in the after-treatment system downstream the TWC converter represents an effective solution to limit the ammonia slip associated with the ammonia production during the rich phases. Indeed, the transient tests shown in this work have shown significant ammonia abatement efficiencies over a commercial ASC dual-layer catalyst working under passive SCR conditions. From an industrial perspective, these results may have a significant impact on managing the operative conditions of natural gas fuelled engines (e.g., using dithering conditions between rich and lean phases). On the other hand, the lumped modelling approach herein developed could be relevant also for industrial researchers who wish to assess the impact of ageing on the activity of Passive SCR and ASC catalysts.

CRediT authorship contribution statement

Nicola Usberti: Data curation, Methodology, Investigation, Formal analysis, Validation, Formal analysis, Writing – original draft, **Sara Ciria:** Data curation, Investigation, Visualization, **Stefano Golini:** Methodology, Validation, Resources, **Gabriella Mancino:** Methodology, Validation, Writing – review & editing, **Edoardo Merlone Borla:** Validation, Supervision, Project administration, **Isabella Nova:** Conceptualization, Resources, Writing – review & editing, **Enrico Tronconi:** Conceptualization, Writing – review & editing, Supervision, Project administration.

Funding

This research was financially supported by FPT Industrial S.p.a., Torino, Italy.

Declaration of Competing Interest

The authors declare that they have no known competing financial interests or personal relationships that could have appeared to influence the work reported in this paper.

Appendix A. Supporting information

Supplementary data associated with this article can be found in the online version at doi:10.1016/j.apcatb.2022.121448.

References

[1] T. Selleri, A.D. Melas, A. Joshi, D. Manara, A. Perujo, R. Suarez-Bertoa, An overview of lean exhaust deNOx aftertreatment technologies and NOx emission regulations in the European Union, Catal 11 (2021), https://doi.org/10.3390/catal11030404.

[2] H. Chen, J. He, X. Zhong, Engine combustion and emission fuelled with natural gas: a review, J. Energy Inst. 92 (2019) 1123–1136, https://doi.org/10.1016/j.joei.2018.06.005.

[3] C. Huang, W. Shan, Z. Lian, Y. Zhang, H. He, Recent advances in three-way catalysts of natural gas vehicles, Catal. Sci. Technol. 10 (2020) 6407–6419, https://doi.org/10.1039/D0CY01320J.

[4] F. Li, Z. Wang, Y. Wang, B. Wang, High-efficiency and clean combustion natural gas engines for vehicles, Automot. Innov. 2 (2019) 284–304, https://doi.org/10.1007/s42154-019-00075-z.

[5] A. Raj, Methane emission control, Johnson Matthey, Technol. Rev. 60 (2016) 228–235, https://doi.org/10.1595/205651316×692554.

[6] D.W. Stanton, Systematic development of highly efficient and clean engines to meet future commercial vehicle greenhouse gas regulations, SAE Int. J. Engines 6 (2013) 1395–1480, https://doi.org/10.4271/2013-01-2421.

[7] C.W. Moore, B. Zielinska, G. Pétron, R.B. Jackson, Air impacts of increased natural gas acquisition, processing, and use: a critical review, Environ. Sci. Technol. 48 (2014) 8349–8359, https://doi.org/10.1021/es4053472.

[8] M. Danielis, S. Colussi, J. Llorca, R.H. Dolan, G. Cavataio, A. Trovarelli, Pd/CeO_2 catalysts prepared by solvent-free mechanochemical route for methane abatement in natural gas fueled vehicles, Ind. Eng. Chem. Res. 60 (2021) 6435–6445, https://doi.org/10.1021/acs.iecr.0c05207.

[9] D. Bounechada, G. Groppi, P. Forzatti, K. Kallinen, T. Kinnunen, Enhanced methane conversion under periodic operation over a Pd/Rh based TWC in the exhausts from NGVs, Top. Catal. 56 (2013) 372–377, https://doi.org/10.1007/s11244-013-9982-8.

[10] T.V. Johnson, A. Joshi, Review of deNOx technology for mobile applications, RSC Catal. Ser. (2018) 1–35, https://doi.org/10.1039/9781788013239-00001.

[11] G.C. Koltsakis, A.M. Stamatelos, Catalytic automotive exhaust aftertreatment, Prog. Energy Combust. Sci. 23 (1997) 1–39, https://doi.org/10.1016/s0360-1285(97)00003-8.

[12] D. Lou, Y. Ren, X. Li, Y. Zhang, X. Sun, Effect of operating conditions and TWC parameters on emissions characteristics of a stoichiometric natural gas engine, Energies 13 (2020), https://doi.org/10.3390/en13184905.

[13] D. Di Maio, C. Beatrice, V. Fraioli, P. Napolitano, S. Golini, F.G. Rutigliano, Modeling of three-way catalyst dynamics for a compressed natural gas engine during lean-rich transitions, Appl. Sci. 9 (2019), https://doi.org/10.3390/app9214610.

[14] Y. Xi, N. Ottinger, Z.G. Liu, The Dynamics of Methane and NOx Removal by a Three-Way Catalyst: A Transient Response Study, 2018 SAE World Congr. Exp. WCX 2018. 2018-April (2018). https://doi.org/10.4271/2018–01-1270.

[15] J. Gong, J. Pihl, D. Wang, M.-Y. Kim, W.P. Partridge, J. Li, M. Cunningham, K. Kamasamudram, N. Currier, A. Yezerets, O_2 dosage as a descriptor of TWC performance under lean/rich dithering in stoichiometric natural gas engines, Catal. Today 360 (2021) 294–304, https://doi.org/10.1016/j.cattod.2020.02.022.

[16] D. Di Maio, C. Beatrice, V. Fraioli, S. Golini, F.G. Rutigliano, Development of a Dedicated CNG Three-Way Catalyst Model in 1-D Simulation Platforms, SAE 14th Int. Conf. Engines Veh. ICE 2019. 2019-Sept, 2019. https://doi.org/10.4271/2019–24-0074.

[17] F. Huang, J. Chen, W. Hu, G. Li, Y. Wu, S. Yuan, L. Zhong, Y. Chen, Pd or PdO: Catalytic active site of methane oxidation operated close to stoichiometric air-to-fuel for natural gas vehicles, Appl. Catal. B Environ. 219 (2017) 73–81, https://doi.org/10.1016/j.apcatb.2017.07.037.

[18] M. Salaün, A. Kouakou, S. Da Costa, P. Da Costa, Synthetic gas bench study of a natural gas vehicle commercial catalyst in monolithic form: On the effect of gas composition, Appl. Catal. B Environ. 88 (2009) 386–397, https://doi.org/10.1016/j.apcatb.2008.10.026.

[19] M. Colombo, I. Nova, E. Tronconi, V. Schmeißer, B. Bandl-Konrad, L. Zimmermann, Experimental and modeling study of a dual-layer (SCR+PGM) NH_3 slip monolith catalyst (ASC) for automotive SCR aftertreatment systems. Part 1. Kinetics for the PGM component and analysis of SCR/PGM interactions, Appl. Catal. B Environ. 142–143 (2013) 861–876, https://doi.org/10.1016/j.apcatb.2012.10.031.

[20] C.D. DiGiulio, J.A. Pihl, J.E.P. II, M.D. Amiridis, T.J. Toops, Passive-ammonia selective catalytic reduction (SCR): understanding NH_3 formation over close-coupled three way catalysts (TWC), Catal. Today 231 (2014) 33–45, https://doi.org/10.1016/j.cattod.2014.01.027.

[21] V.Y. Prikhodko, J.E. Parks, J.A. Pihl, T.J. Toops, Passive SCR for lean gasoline NO_X control: engine-based strategies to minimize fuel penalty associated with catalytic NH_3 generation, Catal. Today 267 (2016) 202–209, https://doi.org/10.1016/j.cattod.2016.01.026.

[22] R. Wunsch, C. Schön, M. Frey, D. Tran, S. Proske, T. Wandrey, M. Kalogirou, J. Schäffner, Detailed experimental investigation of the NOx reaction pathways of three-way catalysts with focus on intermediate reactions of NH_3 and N_2O, Appl. Catal. B Environ. 272 (2020), 118937, https://doi.org/10.1016/j.apcatb.2020.118937.

[23] Q. Zhang, M. Li, S. Shao, G. Li, Ammonia emissions of a natural gas engine at the stoichiometric operation with TWC, Appl. Therm. Eng. 130 (2018) 1363–1372, https://doi.org/10.1016/j.applthermaleng.2017.11.098.

[24] V.Y. Prikhodko, J.A. Pihl, T.J. Toops, J.E. Parks, Passive SCR performance under pseudo-transient cycle: challenges and opportunities for meeting tier 3 emissions, Emiss. Control Sci. Technol. 5 (2019) 253–262, https://doi.org/10.1007/s40825-019-00126-1.

[25] Q. Lin, P. Chen, Y. Vitaly Prikhodko, Model predictive control of a lean-burn gasoline engine coupled with a passive selective catalytic reduction system, in: ASME 2017 Dyn. Syst. Control Conf. DSCC 2017, 2017. https://doi.org/10.1115/DSCC2017–5348.

[26] Q. Lin, P. Chen, V.Y. Prikhodko, Experimental study and model predictive control of a lean-burn gasoline engine coupled with a passive selective catalytic reduction system, J. Dyn. Syst. Meas. Control. Trans. ASME 141 (2019), https://doi.org/10.1115/1.4043269.

[27] M. Colombo, I. Nova, E. Tronconi, V. Schmeißer, B. Bandl-Konrad, L. R. Zimmermann, Experimental and modeling study of a dual-layer (SCR + PGM) NH_3 slip monolith catalyst (ASC) for automotive SCR after treatment systems. Part 2. Validation of PGM kinetics and modeling of the dual-layer ASC monolith, Appl. Catal. B, Environ. 142–143 (2013) 337–343, https://doi.org/10.1016/j.apcatb.2013.05.032.

[28] A. Scheuer, W. Hauptmann, A. Drochner, J. Gieshoff, H. Vogel, M. Votsmeier, Dual layer automotive ammonia oxidation catalysts: experiments and computer simulation, Appl. Catal. B Environ. 111–112 (2012) 445–455, https://doi.org/10.1016/j.apcatb.2011.10.032.

[29] M. Colombo, I. Nova, E. Tronconi, A simplified approach to modeling of dual-layer ammonia slip catalysts, Chem. Eng. Sci. 75 (2012) 75–83, https://doi.org/10.1016/j.ces.2012.02.044.

[30] P. Chen, J. Wang, Estimation and adaptive nonlinear model predictive control of selective catalytic reduction systems in automotive applications, J. Process Control. 40 (2016), https://doi.org/10.1016/j.jprocont.2016.01.005.

[31] Supriyanto, K. Wijayanti, A. Kumar, S. Joshi, K. Kamasamudram, N.W. Currier, A. Yezerets, L. Olsson, Global kinetic modeling of hydrothermal aging of NH_3-SCR over Cu-zeolites, Appl. Catal. B Environ. 163 (2015) 382–392, https://doi.org/10.1016/j.apcatb.2014.07.059.

[32] R. Daya, C. Desai, B. Vernham, Development and validation of a two-site kinetic model for NH_3-SCR over Cu-SSZ-13. Part 1. Detailed global kinetics development based on mechanistic considerations, Emiss. Control Sci. Technol. 4 (2018) 143–171, https://doi.org/10.1007/s40825-018-0095-5.

[33] R. Daya, C. Desai, B. Vernham, Development and validation of a two-site kinetic model for NH_3-SCR over Cu-SSZ-13. Part 2. Full-scale model validation, ASC model development, and SCR-ASC model application, Emiss. Control Sci. Technol. 4 (2018) 172–197, https://doi.org/10.1007/s40825-018-0094-6.

[34] T.K. Torp, B.B. Hansen, P.N.R. Vennestrøm, T.V.W. Janssens, A.D. Jensen, Modeling and optimization of multi-functional ammonia slip catalysts for diesel exhaust aftertreatment, Emiss. Control Sci. Technol. 7 (2021) 7–25, https://doi.org/10.1007/s40825-020-00183-x.

[35] P.S. Dhillon, M.P. Harold, D. Wang, A. Kumar, S.Y. Joshi, Optimizing the dual-layer Pt/Al_2O_3 + Cu/SSZ-13 washcoated monolith: selective oxidation of NH_3 to N_2, Catal. Today 360 (2021) 426–434, https://doi.org/10.1016/j.cattod.2020.01.017.

[36] N. Usberti, F. Gramigni, N.D. Nasello, U. Iacobone, T. Selleri, W. Hu, S. Liu, X. Gao, I. Nova, E. Tronconi, An experimental and modelling study of the reactivity of adsorbed NH_3 in the low temperature NH_3-SCR reduction half-cycle over a Cu-CHA catalyst, Appl. Catal. B Environ. 279 (2020), https://doi.org/10.1016/j.apcatb.2020.119397.

[37] C. Paolucci, A.A. Verma, S.A. Bates, V.F. Kispersky, J.T. Miller, R. Gounder, W. N. Delgass, F.H. Ribeiro, W.F. Schneider, Isolation of the copper redox steps in the standard selective catalytic reduction on Cu-SSZ-13, Angew. Chem. Int. Ed. 53 (2014) 11828–11833, https://doi.org/10.1002/anie.201407030.

[38] F. Gao, D. Mei, Y. Wang, J. Szanyi, C.H.F. Peden, Selective catalytic reduction over Cu/SSZ-13: linking homo- and heterogeneous catalysis, J. Am. Chem. Soc. 139 (2017) 4935–4942, https://doi.org/10.1021/jacs.7b01128.

[39] W. Hu, T. Selleri, F. Gramigni, E. Fenes, K.R. Rout, S. Liu, I. Nova, D. Chen, X. Gao, E. Tronconi, On the redox mechanism of low-temperature NH_3-SCR over Cu-CHA: a combined experimental and theoretical study of the reduction half cycle, Angew. Chem. - Int. Ed. 60 (2021) 7197–7204, https://doi.org/10.1002/anie.202014926.

[40] R.S. Ghosh, P.S. Dhillon, M.P. Harold, D. Wang, Kinetics of NH_3 oxidation on Pt/Al_2O_3: Rate enhancement and NH_3 inhibition, Chem. Eng. J. 417 (2021), 128273, https://doi.org/10.1016/j.cej.2020.128273.

[41] R. Villamaina, S. Liu, I. Nova, E. Tronconi, M.P. Ruggeri, J. Collier, A. York, D. Thompsett, Speciation of Cu cations in Cu-CHA catalysts for NH_3-SCR: effects of SiO_2/Al_2O_3 ratio and Cu-loading investigated by transient response methods, ACS Catal. 9 (2019) 8916–8927, https://doi.org/10.1021/acscatal.9b02578.

[42] M. Colombo, I. Nova, E. Tronconi, V. Schmeißer, B. Bandl-Konrad, L. Zimmermann, $NO/NO_2/N_2O$-NH_3 SCR reactions over a commercial Fe-zeolite catalyst for diesel exhaust aftertreatment: Intrinsic kinetics and monolith converter modelling, Appl. Catal. B Environ. 111 112 (2012) 106–118, https://doi.org/10.1016/j.apcatb.2011.09.023.

[43] T. Selleri, I. Nova, E. Tronconi, An efficient reduced model of NH_3-SCR converters for mobile aftertreatment systems, Chem. Eng. J. 377 (2019), https://doi.org/10.1016/j.cej.2018.09.214.

[44] R. Daya, S.Y. Joshi, J. Luo, R.K. Dadi, N.W. Currier, A. Yezerets, On kinetic modeling of change in active sites upon hydrothermal aging of Cu-SSZ-13, Appl. Catal. B Environ. 263 (2020), https://doi.org/10.1016/j.apcatb.2019.118368.

[45] H. Sjövall, L. Olsson, E. Fridell, R.J. Blint, Selective catalytic reduction of NOx with NH_3 over Cu-ZSM-5-The effect of changing the gas composition, Appl. Catal. B Environ. 64 (2006) 180–188, https://doi.org/10.1016/j.apcatb.2005.12.003.

[46] Y. Xi, N.A. Ottinger, C.J. Keturakis, Z.G. Liu, Dynamics of low temperature N_2O formation under SCR reaction conditions over a Cu-SSZ-13 catalyst, Appl. Catal. B Environ. 294 (2021), https://doi.org/10.1016/j.apcatb.2021.120245.

[47] F. Gramigni, U. Iacobone, N.D. Nasello, T. Selleri, N. Usberti, I. Nova, Review of hydrocarbon poisoning and deactivation effects on Cu- Zeolite, fe-zeolite, and vanadium-based selective catalytic reduction catalysts for nox removal from lean exhausts, Ind. Eng. Chem. Res. 60 (2021) 6403–6420, https://doi.org/10.1021/acs.iecr.0c05894.

[48] R. Villamaina, I. Nova, E. Tronconi, T. Maunula, M. Keenan, The effect of CH_4 on NH_3-SCR over metal-promoted zeolite catalysts for lean-burn natural gas vehicles, Top. Catal. 61 (2018) 1974–1982, https://doi.org/10.1007/s11244-018-1004-4.

[49] C. Paolucci, I. Khurana, A.A. Parekh, S. Li, A.J. Shih, H. Li, J.R. Di Iorio, J. D. Albarracin-Caballero, A. Yezerets, J.T. Miller, W.F. Schneider, R. Gounder, Dynamic multinuclear sites formed by mobilized copper ions in NO_x selective

catalytic reduction, Science 357 (2017) 898–903, https://doi.org/10.1126/science.aan5630.
[50] T.V.W. Janssens, H. Falsig, L.F. Lundegaard, P.N.R. Vennestrøm, S.B. Rasmussen, P. G. Moses, F. Giordanino, E. Borfecchia, K.A. Lomachenko, C. Lamberti, S. Mossin, P. Beato, A consistent reaction scheme for the selective catalytic reduction of nitrogen oxides with ammonia, ACS Catal. 5 (2015) 2832–2845, https://doi.org/10.1021/cs501673g.
[51] F. Gramigni, N.D. Nasello, N. Usberti, U. Iacobone, T. Selleri, W. Hu, S. Liu, X. Gao, I. Nova, E. Tronconi, Transient kinetic analysis of low-temperature NH_3-SCR over Cu-CHA catalysts reveals a quadratic dependence of Cu reduction rates on cuII, ACS Catal. 11 (2021) 4821–4831, https://doi.org/10.1021/acscatal.0c05362.
[52] R.S. Ghosh, M.P. Harold, D. Wang, Selective oxidation of NH_3 in a Pt/Al_2O_3@Cu/ZSM-5 core-shell catalyst: modeling and optimization, Chem. Eng. J. 418 (2021), 129065, https://doi.org/10.1016/j.cej.2021.129065.
[53] F. Cabello Galisteo, R. Mariscal, M. López Granados, J.L.G. Fierro, R.A. Daley, J. A. Anderson, Reactivation of sintered Pt/Al_2O_3 oxidation catalysts, Appl. Catal. B Environ. 59 (2005) 227–233, https://doi.org/10.1016/j.apcatb.2005.02.004.
[54] B.-S. Kim, H. Jeong, J. Bae, P.S. Kim, C.H. Kim, H. Lee, Lean NOx trap catalysts with high low-temperature activity and hydrothermal stability, Appl. Catal. B Environ. 270 (2020), https://doi.org/10.1016/j.apcatb.2020.118871.
[55] J. Yang, V. Tschamber, D. Habermacher, F. Garin, P. Gilot, Effect of sintering on the catalytic activity of a Pt based catalyst for CO oxidation: Experiments and modeling, Appl. Catal. B Environ. 83 (2008) 229–239, https://doi.org/10.1016/j.apcatb.2008.02.018.